EBioMedicine 27 (2018) 225–236

Contents lists available at ScienceDirect

EBioMedicine

journal homepage: www.ebiomedicine.com

Research paper

A Vascular Endothelial Growth Factor-Dependent Sprouting Angiogenesis Assay Based on an *In Vitro* Human Blood Vessel Model for the Study of Anti-Angiogenic Drugs

Joris Pauty [a,b,c], Ryo Usuba [a], Irene Gayi Cheng [d], Louise Hespel [e], Haruko Takahashi [a], Keisuke Kato [f], Masayoshi Kobayashi [f], Hiroyuki Nakajima [g], Eujin Lee [a], Florian Yger [h], Fabrice Soncin [c,i,*], Yukiko T. Matsunaga [a,b,c,**,1]

[a] Center for International Research on Integrative Biomedical Systems (CIBiS), Institute of Industrial Science, The University of Tokyo, 4-6-1 Komaba, Meguro-ku, Tokyo 153-8505, Japan
[b] LIMMS/CNRS-IIS UMI 2820, Institute of Industrial Science, The University of Tokyo, 4-6-1 Komaba, Meguro-ku, Tokyo 153-8505, Japan
[c] CNRS/IIS/COL/Université Lille 1 SMMiL-E project, CNRS Délégation Nord-Pas de Calais et Picardie, 2 rue de Canonniers, Lille, Cedex 59046, France
[d] Department of Bioengineering, Clemson University, 118 Engineering Service Dr., Clemson, SC 29634, USA
[e] Ecole Normale Supérieure-PSL Research University, Département de Chimie, Sorbonne Universités, UPMC Université Paris 06, CNRS UMR 8640 PASTEUR, 24 rue Lhomond, 75005 Paris, France
[f] R&D Department 1, SCREEN Holdings Co., Ltd., 322 Furukawa-cho, Hazukashi, Fushimi-ku, Kyoto 612-8486, Japan
[g] Department of Cell Biology, National Cerebral and Cardiovascular Center Research Institute, Suita, Japan
[h] LAMSADE, CNRS UMR 7243, Université Paris-Dauphine, PSL Research University, 75016 Paris, France
[i] Université Lille, CNRS, Institut Pasteur de Lille, UMR 8161 - M3T, F-59000 Lille, France

ARTICLE INFO

Article history:
Received 6 November 2017
Received in revised form 6 December 2017
Accepted 14 December 2017
Available online 20 December 2017

Keywords:
Angiogenesis inhibitors
DLL4
Human umbilical vein endothelial cell
In vitro 3D model
Microvessel
Notch
Sorafenib
Sprouting angiogenesis
Sunitinib
Vascular endothelial growth factor

ABSTRACT

Angiogenesis is the formation of new capillaries from pre-existing blood vessels and participates in proper vasculature development. In pathological conditions such as cancer, abnormal angiogenesis takes place. Angiogenesis is primarily carried out by endothelial cells, the innermost layer of blood vessels. The vascular endothelial growth factor-A (VEGF-A) and its receptor-2 (VEGFR-2) trigger most of the mechanisms activating and regulating angiogenesis, and have been the targets for the development of drugs. However, most experimental assays assessing angiogenesis rely on animal models. We report an *in vitro* model using a microvessel-on-a-chip. It mimics an effective endothelial sprouting angiogenesis event triggered from an initial microvessel using a single angiogenic factor, VEGF-A. The angiogenic sprouting in this model is depends on the Notch signaling, as observed *in vivo*. This model enables the study of anti-angiogenic drugs which target a specific factor/receptor pathway, as demonstrated by the use of the clinically approved sorafenib and sunitinib for targeting the VEGF-A/VEGFR-2 pathway. Furthermore, this model allows testing simultaneously angiogenesis and permeability. It demonstrates that sorafenib impairs the endothelial barrier function, while sunitinib does not. Such *in vitro* human model provides a significant complimentary approach to animal models for the development of effective therapies.

1. Introduction

The vascular system is a complex network made of tubular structures which distribute blood-contained nutrients, oxygen, and cells to and from most organs throughout the body. As a result, it is deeply involved in maintaining homeostasis of the living body. In adults, the formation of the vascular system is mainly ensured by the emergence of new capillaries from existing vessels; an event known as "sprouting angiogenesis". Sprouting angiogenesis is triggered by the lack of oxygen in growing or ischemic tissues (hypoxia) which release angiogenic factors such as vascular endothelial growth factors (VEGF) into the environment. Established neighboring vessels respond to these signals by sprouting new blood vessels that extend in the gradient of angiogenic factors. Within these sprouting capillaries, tip-cells respond to VEGF

Abbreviations: 3D, three-dimensional; BSA, bovine serum albumin; CLSM, confocal laser scanning microcopy; DLL4, Delta-like protein 4; DMSO, dimethyl sulfoxide; ECM, extracellular matrix; EGM-2, endothelial cell growth medium-2; HUVEC, human umbilical vein endothelial cells; kDa, kilodalton; LSFM, light sheet fluorescence microscopy; mRNA, messenger ribonucleic acid; NOCTH1, Neurogenic locus notch homolog protein 1; PBS, phosphate buffered saline; PDMS, polydimethylsiloxane; PFA, paraformaldehyde; siRNA, small interfering ribonucleic acid; UV, ultraviolet; VE-Cad, vascular-endothelial cadherin; VEGF, vascular endothelial growth factor; VEGFR-2, VEGF receptor-2.

* Correspondence to: F. Soncin, CNRS UMR 8161, 1 rue du Pr Calmette, 59000 Lille, France.

** Correspondence to: Y. T. Matsunaga, Institute of Industrial Science, The University of Tokyo, 4-6-1 Komaba, Meguro-ku, Tokyo 153-8505, Japan.

E-mail addresses: fabrice.soncin@inserm.fr (F. Soncin), mat@iis.u-tokyo.ac.jp (Y.T. Matsunaga).

[1] Lead contact.

https://doi.org/10.1016/j.ebiom.2017.12.014

and form characteristic protruding and actin-rich filopodia. Tip-cells do not proliferate, but migrate toward the source of VEGF, thus giving directionality to an angiogenic sprout. Stalk-cells proliferate behind the leading tip-cells and allow for the extension of the angiogenic sprouts (Ribatti and Crivellato, 2012). During the extension of the capillary sprouts, the formation of the vessel lumen in stalk-cells is ensured by endothelial cytoskeleton rearrangements in response, in part, to hydrodynamic forces (Gebala et al., 2016; Charpentier and Conlon, 2014).

The VEGF family of proteins includes five sub-types in vertebrates; VEGF-A, -B, -C, -D and placental growth factor (PlGF). These factors play crucial roles in the formation and maintenance of blood and lymphatic vasculatures through the activation of specific tyrosine kinases VEGF-receptors (VEGF-R). VEGFR-2 is the most studied receptor in human blood vascular endothelial cells activated by VEGF-A and the VEGF-A/VEGFR-2 pathway plays essential roles in angiogenesis. This pathway is involved in the initial determination of the tip/stalk-cell fate through the Delta-like protein 4 (DLL4)/Neurogenic locus notch homolog protein 1 (NOTCH1) (Simons et al., 2016; Hellstrom et al., 2007). VEGF-A binds to its receptor VEGFR-2 on the membrane of endothelial cells, leading to its dimerization. It triggers the activation of the intracellular kinase domain of VEGFR-2, which initiates a signaling cascade leading the responding cell to become a tip-cell and to express DLL4 at its surface. DLL4 interacts with its receptor NOTCH1 on the surface of adjacent endothelial cells. This activates a gamma-secretase complex, causing the downstream activation of molecular pathways that result in a decrease of sensitivity to VEGF-A and stimulates endothelial proliferation, therefore shifting cells toward the stalk-cell fate (Simons et al., 2016; Blanco and Gerhardt, 2013). Upon activation of this system, sprouts form and progress toward the hypoxic tissues (Fig. 1). Angiogenesis takes place in pathological conditions such as inflammation, vaso-proliferative retinopathies, and cancers (Potente et al., 2011; Carmeliet and Jain, 2000) and it was proposed during the 1970s that angiogenesis inhibitors could be designed as anticancer drugs (Folkman, 1971). This eventually led to the development of molecules targeting VEGF-A, its receptors, or downstream effectors of this pathway. Some were approved for clinical use, such as bevacizumab (Avastin), sunitinib (Sutent) and sorafenib (Nexavar), which were among the first available targeted therapies (Niu and Chen, 2010; Carmeliet and Jain, 2011a).

To study angiogenesis and develop more specific therapies, several experimental models were developed using 2D cell culture and animal models (Staton et al., 2004). Recently, sophisticated *in vitro* models have been created to study sprouting angiogenesis of human endothelial cells in a 3D environment simulating the extracellular matrix (ECM). For example, the microbead assay consists in growing endothelial cells to confluence on microbeads which are then embedded into a fibrin gel. Upon treatment with pro-angiogenic factors, capillary formation can be induced (Nakatsu et al., 2003). However, this technique has several limitations, such as the lack of a parent vessel with a lumen. Secondly, although human endothelial cells have been used in this assay, the presence of fibroblasts was required to maintain growth and promote lumen formation. The presence of another cell type in such assay complicates the technique and the analysis of specific processes. For example, it may be difficult to study the direct effect of any drug on endothelial cell sprouting when fibroblasts may also respond to such a drug and trigger an indirect effect. Moreover, due to the spherical structure of the beads, the local inhibition of sprouting in the neighborhood

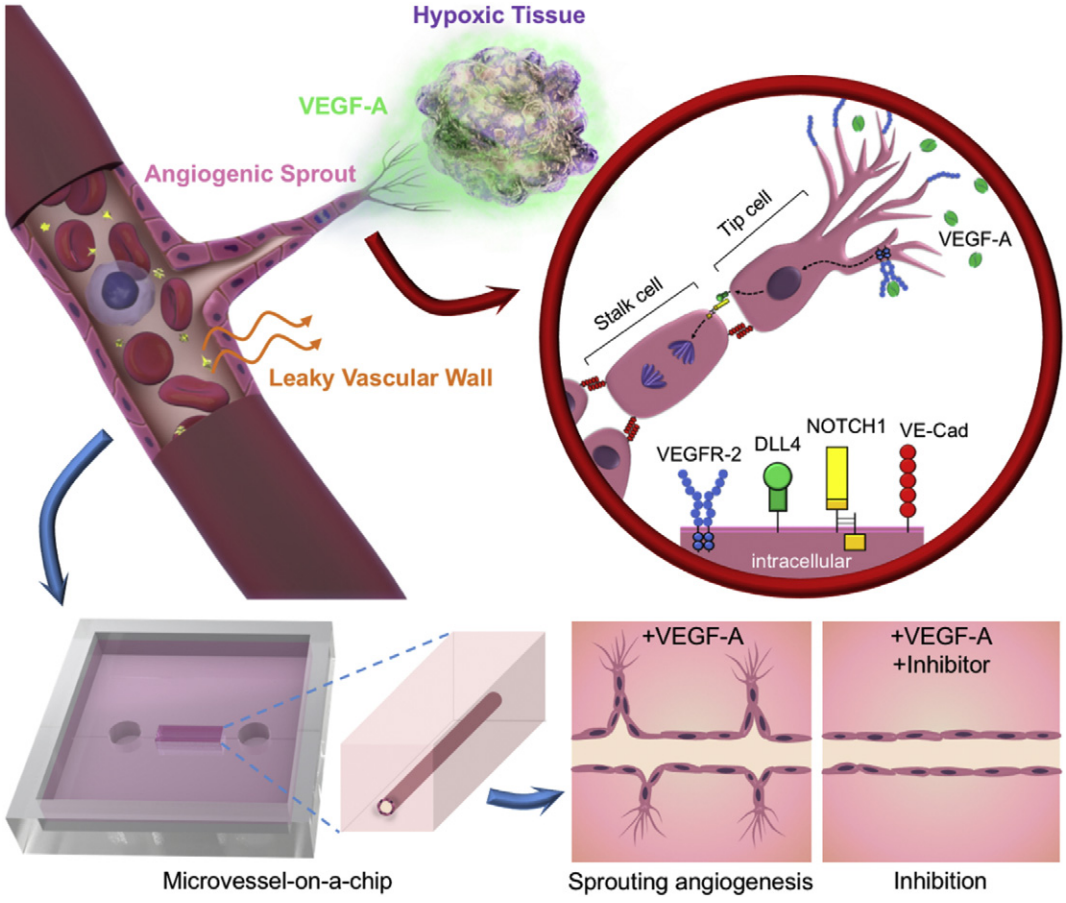

Fig. 1. Concept of the present study: VEGF-induced angiogenesis-on-a-chip for gene and inhibitor study. (Top) *In vivo*, the DLL4/NOTCH1 pathway orients the endothelial cell fate within an angiogenic sprout. The tip-cell migrates and expresses DLL4, while the stalk-cell is inhibited in its migration by the DLL4/NOTCH1 interaction which rather triggers cell proliferation. (VE-Cad: VE-cadherin) (Bottom) Concept of the model: a human microvessel is fabricated on a PDMS chip within a collagen gel scaffold and used to study VEGF-A-induced angiogenesis, permeability and angiogenic inhibitors effects.

of an existing sprout cannot be easily studied, and until recently such studies relied on the zebrafish animal model (Yokota et al., 2015). With the development of microengineering, new *in vitro* models could be created. These models use technologies such as microfluidics or tissue engineering (Nguyen et al., 2013; Kim et al., 2013; Tourovskaia et al., 2014; Zheng et al., 2017). The microfluidic models share common limitations with the microbead assay; namely, the absence of a parent vessel or the need for coculture. Such a model was recently reported which relied on the use of co-cultures of endothelial cells and fibroblasts within a fibrin matrix with no establishment of an initial endothelial capillary (Zheng et al., 2017). The endothelial sprouting/migration events observed in these conditions were induced by fibroblasts and sensitive to Notch inhibitors. However, the need of a second cell line to induce such events makes it very difficult to study the precise effects of unique growth and regulatory factors which initiate and regulate sprouting angiogenesis.

In the present study, we used a tissue-engineering approach to develop a model enabling the specific study of the first steps of sprouting angiogenesis induced by a single angiogenic factor such as VEGF-A, taken as a model factor. We created an initial microvessel contained within a collagen gel in a polydimethylsiloxane (PDMS) chip, which, when treated with VEGF-A alone, undergoes morphological changes while maintaining its inner lumen and eventually forms distinct angiogenic sprouts with minimal unicellular migration. This model allows for the use of genetically-altered endothelial cells and allowed us to demonstrate the regulating role of the DLL4/NOTCH1 pathway by the use of ribonucleic acid (RNA) interference. Furthermore, we developed fluorescence microscopy and optical coherence tomography in order to visualize and quantify the sprouting events. We also assessed the potential use of this model to investigate angiogenic inhibitors by developing an analytical method which enables conclusive observations from phase-contrast images, therefore preserving the samples. Finally, we setup conditions to study the effects of clinically-used angiogenic inhibitors on endothelial permeability and barrier function.

2. Materials and Methods

2.1. Cell Culture

Primary human umbilical vein endothelial cells (HUVEC) and Endothelial Cell Growth Medium-2 BulletKit (EGM-2) were obtained from Lonza (Basel, Switzerland), and Endothelial Cell Growth Medium (ECGM) purchased from Promocell (Heidelberg, Germany). 10× Dulbecco's-phosphate buffered saline (PBS) (−) (2 g/L KCl, 80 g/L NaCl, 2 g/L KH_2PO_4, 11.5 g/L Na_2HPO_4) was from Wako Pure Chemical Industries, Ltd. (Osaka, Japan). 5 mL polystyrene round-bottom tube with cell-strainer cap (12 × 77 mm) and 0.5% Trypan blue stain solution were obtained from Corning Falcon (Corning, NY, USA) and Nacalai Tesque, Inc. (Kyoto, Japan), respectively.

In order to reduce the number of passages and to use the cells at the same passage when preparing microvessels, primary HUVEC were thawed upon reception, amplified for two passages in EGM-2 and frozen again. When fabricating microvessels, cells were thawed in EGM-2, seeded in 21 cm^2 culture dishes, cultured at 37 °C in a humidified atmosphere of 5% CO_2/95% air, and used at 70–80% confluence. Cells were harvested by rinsing once with PBS, incubating with 0.25% trypsin-EDTA solution for 3 min at 37 °C in 5% CO_2/95% air and collected in ECGM. Cells were passed through a 35 μm cell strainer to dissociate cell aggregates; stained with Trypan Blue and live cells were counted using a hemocytometer.

2.2. DLL4 Gene Silencing by RNA Interference

HUVEC were seeded on 9.6 cm^2-well plates. When cells reached 50–60% confluence, they were rinsed once and 450 μL of warmed OptiMEM (Thermo Fisher Scientific, Waltham, MA, USA) was added. 50 nM of siRNA targeting the DLL4 mRNA (ON-TARGETplus smartpool DLL4 #L-010490-00-0005, Dharmacon, Inc., Lafayette, CO, USA) or of non-targeting siRNA (siCtl, ON-TARGETplus Non-targeting siRNA #D-001810-01-20, Dharmacon) were incubated with Lipofectamine RNAiMAX (Thermo Fisher Scientific) for 20 min at 25 °C, then transferred onto cells. After 6 h of incubation at 37 °C in 5% CO_2/95% air, medium was changed for EGM-2 and cells cultured for 24 h. Culture medium was then changed for ECGM and cells were cultured for an additional 24 h before being used to make microvessels. Cells not used for microvessel fabrication were used for RNA extraction and DLL4 silencing was validated by RT-qPCR using TaqMan method (Sup. Method 1).

2.3. Fabrication of the Microvessel-on-a-Chip

2.3.1. Polydimethylsiloxane Chips

The chips used in this study and their fabrication method have been previously described (Pauty et al., 2017). Briefly, polydimethylsiloxane (PDMS)-based chips (25 mm × 25 mm × 5 mm: width × length × height) which included needle inserting channels (300 μm in diameter) on both sides were prepared and kindly gifted by Dai Nippon Printing Ltd. (Tokyo, Japan). A mold was prepared using a 3D printer and its surface treated with a release agent. A mixture of PDMS and a curing agent (SILPOT 184; Dow Corning Toray Co., Ltd., Tokyo, Japan) at a ratio of 10:1 (w/w) was cast on the mold equipped with 300-μm-diameter microneedles and cured at 37 °C overnight. The concave PDMS device was then peeled off the mold. The PDMS device and a glass coverslip thickness No.1 0.12–0.17 mm, Matsunami, (Osaka, Japan) were then treated with O_2 plasma (PDC-32G; Harrick Plasma (Ithaca, NY, USA)) for 60 s and bonded at 150 °C for 30 min. The PDMS device was checked for leaks with 70% ethanol (Kanto Chemical) for 30 min before sterilization by ultraviolet (UV)-light exposure for one hour under a cell culture hood.

2.3.2. Fabrication of a Microvessel

Cellmatrix Type I-A (3 mg/mL, pH 3, collagen derived from porcine tendons by acid extraction) and 10× Hank's were obtained from Nitta Gelatin Co., Ltd. (Osaka, Japan) and Sigma-Aldrich Co., Ltd. (Saint Louis, MO, USA), respectively. The collagen buffer used for the neutralization of the collagen solution contains 262 mM $NaHCO_3$, 20 mM HEPES and 0.05 N NaOH. NaOH and $NaHCO_3$ were obtained from Kanto Chemical Co., Inc. (Tokyo, Japan), and HEPES from Sigma-Aldrich. Acupuncture needles (No.02, 0.20 mm × 30 mm, J type) were from Seirin Co., Ltd. (Shizuoka, Japan). Bovine serum albumin (BSA) and dextran from *Leuconostoc* spp. (Mr 450,000–650,000) were from Sigma-Aldrich.

First, the PDMS chip was treated with O_2 plasma for 1 min and then sterilized by UV-light exposure for 5 min under a cell culture hood. An acupuncture needle (200 μm in diameter) was then coated with 1% BSA in PBS solution at 25 °C for at least 5 min to prevent collagen adhesion, dried, and sterilized by UV-light exposure under a cell culture hood. The neutralized collagen solution was prepared on ice by mixing Cellmatrix Type I-A collagen solution, 10× Hank's buffer, and 10× collagen buffer (volume ratio 8:1:1) following manufacturer's protocol. Next, ice-cold neutralized collagen solution was introduced into both wells and in the microvessel chamber; and the BSA-coated acupuncture needle inserted through the PDMS channel (Fig. 2). The excess of collagen was carefully withdrawn from the wells. The device was then incubated at 37 °C in 5% CO_2/95% air for 90 min to allow the collagen to gel and a hollow channel was created by withdrawing the needle. To prevent leakage of the chip through the PDMS channels used to insert the needle, two short needles (300 μm in diameter, 8 mm long) were then inserted in the PDMS channels located between the wells and the external edges of the device. HUVEC were harvested and resuspended in ECGM containing 3% dextran at a density of 1×10^7 cells/mL and 20,000 cells were added at each opening of the collagen channel. After checking for the effective entry of cells into the collagen channel, the chip was flipped upside-down and incubated at 37 °C in 5% CO_2/95%

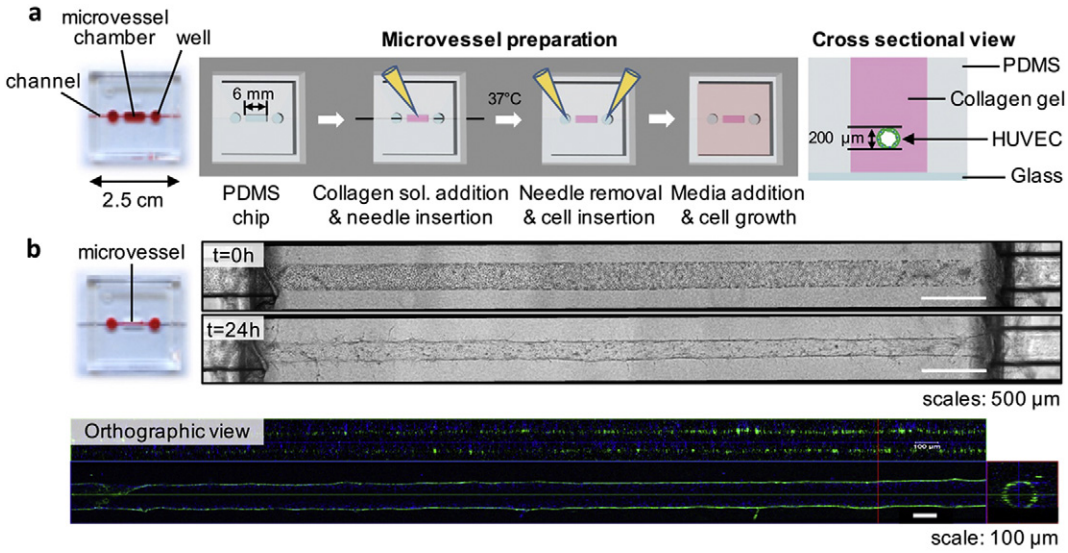

Fig. 2. Fabrication of the *in vitro* human microvessel using a PDMS chip. (a) Schematic of the method for fabricating the 3D *in vitro* model of a human microvessel. (collagen sol.: collagen solution) (b) Phase-contrast and CLSM images of a microvessel. The orthographic view shows the lumen (green: actin cytoskeleton, blue: nucleus).

air. After 10 min, the chip was flipped back and incubated for an additional 5 min in the same conditions. 1 mL of warm medium was then added and the chip was further incubated for 4 h. Finally, the medium was changed and cell culture was maintained at 37 °C in 5% CO_2/95% air with medium renewal every other day.

2.4. VEGF-Dependent Angiogenesis Model

Recombinant human VEGF-A_{165} and PBS, 4% (w/w) paraformaldehyde (PFA) were purchased from Wako. The kinase inhibitors sorafenib and sunitinib were from Selleck Chemicals LLC (Houston, TX, USA).

Microvessels were prepared and cells cultured in ECGM (endothelial cell basal medium supplemented with 2% fetal calf serum, 0.4% endothelial cell growth supplement, 0.1 ng/mL recombinant human epidermal growth factor, 1 ng/mL recombinant human basic fibroblast growth factor, 90 µg/mL heparin and 1 µg/mL hydrocortisone) rather than EGM-2 to ensure that no VEGF-A was present in the controls. 24 h after fabrication of the initial microvessel, the medium was changed for medium containing 50 ng/mL VEGF-A. VEGF-A-containing medium was renewed every other day, for 10 days. Microscopic images were taken using an inverted phase-contrast microscope Observer Z1 (Carl Zeiss, GmbH, Oberkochen, Germany) equipped with a 20× objective lens (LD Plan-NeoFluar 20×/0.4 Korr Ph2 M27) and the ZEN 2 blue edition software (version 2.0.0.0, 64 bit, Carl Zeiss). At the end of the experiments, microvessels were fixed in PBS, 4% paraformaldehyde (PFA) for 30 min at 25 °C, and stored in PBS at 4 °C.

For the study of the angiogenic inhibitors, 24 h after fabrication, microvessels were treated with 1 µM of sorafenib, 1 µM of sunitinib or 0.01% DMSO and with or without 50 ng/mL VEGF-A in ECGM. Medium was renewed every other day. After 10 days, phase-contrast images were taken using an inverted phase-contrast microscope Observer Z1 (Carl Zeiss) and computationally analyzed by the directional pixel variance method (described later). Microvessels were fixed as previously described.

2.5. Immunofluorescence on a Microvessel to Visualize Cell-Cell Junctions

Triton X-100 was purchased from Sigma-Aldrich. The primary antibody targeting vascular endothelial (VE)-cadherin (Rabbit mAb, D87F2) was from Cell Signaling Technology, Inc. (Danvers, MA, USA). The Alexa Fluor 488 phalloidin, secondary antibody Alexa Fluor 568 goat anti-rabbit, and Hoechst 33342 were from Thermo Fisher Scientific, Co. (Waltham, MA, USA).

The fixed microvessels were permeabilized in PBS, 0.5% Triton X-100 for 5 min at 25 °C. Blocking was performed for overnight at 4 °C with PBS, 1% BSA (blocking solution). Samples were then incubated overnight at 4 °C with anti-VE-cadherin antibody (1:200) in blocking solution. After 6 washes with PBS, samples were incubated for 2 h at 25 °C with Alexa Fluor 568 goat anti-rabbit antibody and Alexa Fluor 488 phalloidin for actin staining in PBS (1:200). After washing with PBS, nuclei were stained by incubating the cells for 15 min at 25 °C with Hoechst 33342 diluted 1:1000 in PBS. After several washes with PBS, the chip was stored at 4 °C until imaging.

Images were taken using a confocal laser scanning microscope (CLSM, Laser Scanning Microscope 700, LSM 700, Carl Zeiss) equipped with a 40× water-immersion detection objective lens (LD C-Apochromat 40×/1.1 W Korr M27). Phalloidin, VE-cadherin, and Hoechst 33,342 were detected using 488-, 555- and 405-nm-wavelength lasers, respectively. Maximum intensity projection (MIP) and orthographic view images were obtained with the ZEN 2 blue edition software (version 2.0.0.0, 64 bit, Carl Zeiss). Light-sheet fluorescence microscopy (LSFM) imaging was performed with a Lightsheet Z.1 system (Carl Zeiss) equipped with a 20× water-immersion detection objective lens (W Plan Apochromat, NA 1.0), dual sided 10× illumination objective lenses (LSMF, NA 0.2), a pco.edge scientific CMOS camera (PCO) and ZEN software.

2.6. Preservative Imaging Methods and Image Analysis of Microvessels to Assess Sprout Features and Responsiveness to Angiogenic Inhibitors

2.6.1. High Resolution Optical Coherence Tomography for 3D Imaging of Microvessel and Measurement of Angiogenic sprout's Features

OCT setup was previously described (Takahashi et al., 2017). Slight changes were made in the setup to increase the optical resolution to 3 µm: the voxel size was 2 × 2 × 2 µm and the beam diameter was 10 µm. The average data acquisition window was 700 × 700 × 700 µm (h × w × l) correlating with 351 scans per axis in 30 min.

For 3D images, original images obtained by the OCT system were processed using ImageJ (National Institute of Health) to reduce the noise due to collagen gel, by subsequently applying the filters: (i) 3D maximum, (ii) 3D Gaussian low-pass, (iii) 2D FFT band-pass, and (iv) 3D Gaussian low-pass. Images were then converted into binary images and 3D images were constructed using the ImageJ plugin: 3D viewer.

In order to measure the features of the angiogenic sprouts, the following method was applied in ImageJ: (i) the gray image of a sprout was changed to a 3D binary image; (ii) volume and surface were calculated using the 3D Objects Counter function; (iii) 3D binary image of the sprout was then skeletonized by applying the plugin Skeletonize(2D/3D); (iv) the length of sprout was measured by applying Analyze Skeleton(2D/3D); (v) finally, the average diameter of the sprout was calculated using its volume and length with the assumption that its cross section was circular.

2.6.2. Method of Directional Pixel Variance to Assess the Responsiveness of Microvessel to VEGF-A

The phase-contrast image was processed with ImageJ. First, the background was removed by processing the image as follows: (i) rotating the image to orient microvessels vertically, (ii) changing the gray image to a binary image, (iii) dividing the binary image by 255 using the ImageJ's function Divide–the background becomes zero and the edges of the microvessel become one, (iv) multiplying the original image with the binary image by using the ImageJ's function Image Calculator–the background is thus given a value zero while the value for the edges of the microvessel remains unchanged. Then, using the rectangular selection tool, a region of interest was selected excluding both extremities of the microvessels, because these regions sometimes formed improperly due to the connection point between the collagen matrix and PDMS channel. The coordinates of the rectangular selection were incorporated into a macro (Sup. Method 2) which calculates the mean of the directional pixel variance by performing the following steps: (i) creating the profile of the region of interest by using the ImageJ's function Plot Profile, (ii) making the difference of pixel intensity between every horizontal line of the rectangular area and computing the profile which gave a set of horizontal line of residuals, (iii) averaging the square of the residuals to give a number called directional pixel variance. Finally, the average directional pixel variance and standard deviation for each experimental condition was calculated. The results are presented as a ratio to the untreated condition.

2.7. Permeability Assay to Investigate the Endothelial Barrier Function after Treatment With Angiogenic Inhibitors

Rhodamine-conjugated *Ulex europaeus* Agglutinin 1 (UEA-1, 2 mg/mL) and Fluorescein isothiocyanate-dextran (FITC-dextran, 70 kDa) were obtained from Vector Laboratories, Inc. (Burlingame, CA, USA) and Sigma-Aldrich, respectively.

The microvessels were stained with 20 μg/mL rhodamine-conjugated UEA-1 in ECGM for 30 min. The microchips were then set up on a confocal microscope LSM700 (Carl Zeiss) in an incubation chamber that maintained 37 °C in a humidified 5% CO_2/95% air atmosphere (INU Incubation System for Microscopes–model WSKM, Tokai Hit Co., Fujinomiya, Japan). Images were taken using the CLSM equipped with a 10× observation lens (N-Achroplan 10×/0.25 M27). The rhodamine-conjugated UEA-1 staining was detected with the 555-nm-wavelength laser and used to focus the microscope. Then, 15 μL of 100 μg/mL FITC-dextran (70 kDa) in ECGM solution was introduced and imaging was performed by detecting the fluorescence of FITC with the 488-nm-wavelength laser and an optical section of 77.8 μm. Permeability was quantified through the mean fluorescence intensity of the FITC-dextran detected within two regions of interest ("mean ROI") outside a microvessel within the collagen, as previously reported (Pauty et al., 2017). Briefly, for each microvessel, two regions of interest of 0.2 mm × 2.5 mm (0.5 mm^2) were drawn using the ZEN 2012 SP1 black edition software (version 8.1.0.484, 64 bit, Carl Zeiss), aligned along the edges of the microvessel and centered on the middle of it. The mean ROIs given by the ZEN software for the two boxes were added to give the final fluorescence intensity value. The average fluorescence intensity and standard deviation for each experimental condition was calculated. The results are presented as a ratio to the average fluorescence of the untreated condition.

3. Results

3.1. VEGF-Induced Sprouting Angiogenesis

In this study, we aimed at developing a model where we could induce sprouting angiogenesis from an established endothelial cell microvessel (Fig. 1). By seeding primary human umbilical vein endothelial cells (HUVEC) into a collagen gel tubular scaffold within a PDMS chip, we first created the initial *in vitro* 3D microvessel (HUVEC, Fig. 2, (Pauty et al., 2017)). We then set up conditions in order to maintain a stable and non-sprouting microvessel that could be stimulated into sprouting angiogenesis at will following stimulation with angiogenic factors such as VEGF-A. In order to setup initial conditions which avoided the use of VEGF-A found in most endothelial cell culture media, VEGF-free endothelial cell growth medium (ECGM) specifically designed for the optimal growth and survival of HUVEC (see Materials and Methods for the detailed composition) was used. The stable, non-sprouting, initial microvessel could be maintained for up to 10 days in these conditions without showing signs of angiogenesis (Fig. 3a & b). In order to induce sprouting angiogenesis, VEGF-A (50 ng/mL) was added to the culture medium 24 h after fabricating microvessels in ECGM, a concentration consistent with other published works (Heiss et al., 2015). Upon this stimulation, the emergence and progression of angiogenic sprouts was observed and monitored by phase-contrast microscopy. Under these conditions, endothelial sprouts emerged at day 4, became clearly distinguishable at day 6, and extended until the end of the experiment at day 10 (Fig. 3c).

Samples were then fixed and the actin cytoskeleton was immunostained to visualize the morphology of the sprouts and to assess their structure. Most importantly, CLSM orthographic view images showed the presence of a lumen connecting the parent vessel with the newly formed angiogenic sprouts, a typical feature of sprouting capillaries *in vivo* (Charpentier and Conlon, 2014). Furthermore, actin cytoskeleton staining highlighted filopodia protrusion from the cells located at the tips of the sprouts, strongly resembling the tip-cell morphology observed *in vivo* (Fig. 3d, (Geudens and Gerhardt, 2011)).

The induction of sprouts by VEGF-A, the presence of a lumen within the sprouts, and filopodia on the leading cells, all together, show that the sprouts formed in this model are morphologically similar to *bona fide* angiogenic *in vivo* sprouts. This suggests that the established model reconstitutes, at least in part, the events leading to capillary formation by endothelial cells during sprouting angiogenesis.

3.2. Control of Sprouting Angiogenesis by the DLL4/NOTCH1 Signaling

In order to further validate the biological relevance of this model and to demonstrate its possible use for investigating gene function, HUVEC were genetically modified using RNA silencing before making microvessels. The *DLL4* gene was targeted because of its important role in VEGF-A-induced angiogenic sprout formation *in vivo*. HUVEC were transfected with a siRNA targeting *DLL4* (siDLL4) or a non-targeting siRNA (siControl, siCtl) in culture dishes. After 48 h, the transfected cells were seeded as microvessels which were then treated with or without 50 ng/mL VEGF-A for the next 10 days. Gene silencing was effective at 48 h as seen at the RNA and protein levels (Fig. S1).

As seen with unmodified HUVEC, the microvessels made of genetically-modified HUVEC with a siControl (HUVEC-siCtl) showed smooth edges when untreated, and rough edges with angiogenic sprouts when treated with VEGF-A for 10 days (Fig. 4a); therefore, demonstrating that the transfection method did not generally affect the behavior of HUVEC in the model. Interestingly, HUVEC genetically-modified with siRNA targeting *DLL4* (HUVEC-siDLL4) did not form a stable microvessel in the absence of VEGF-A but rather adopted a migratory and collagen-

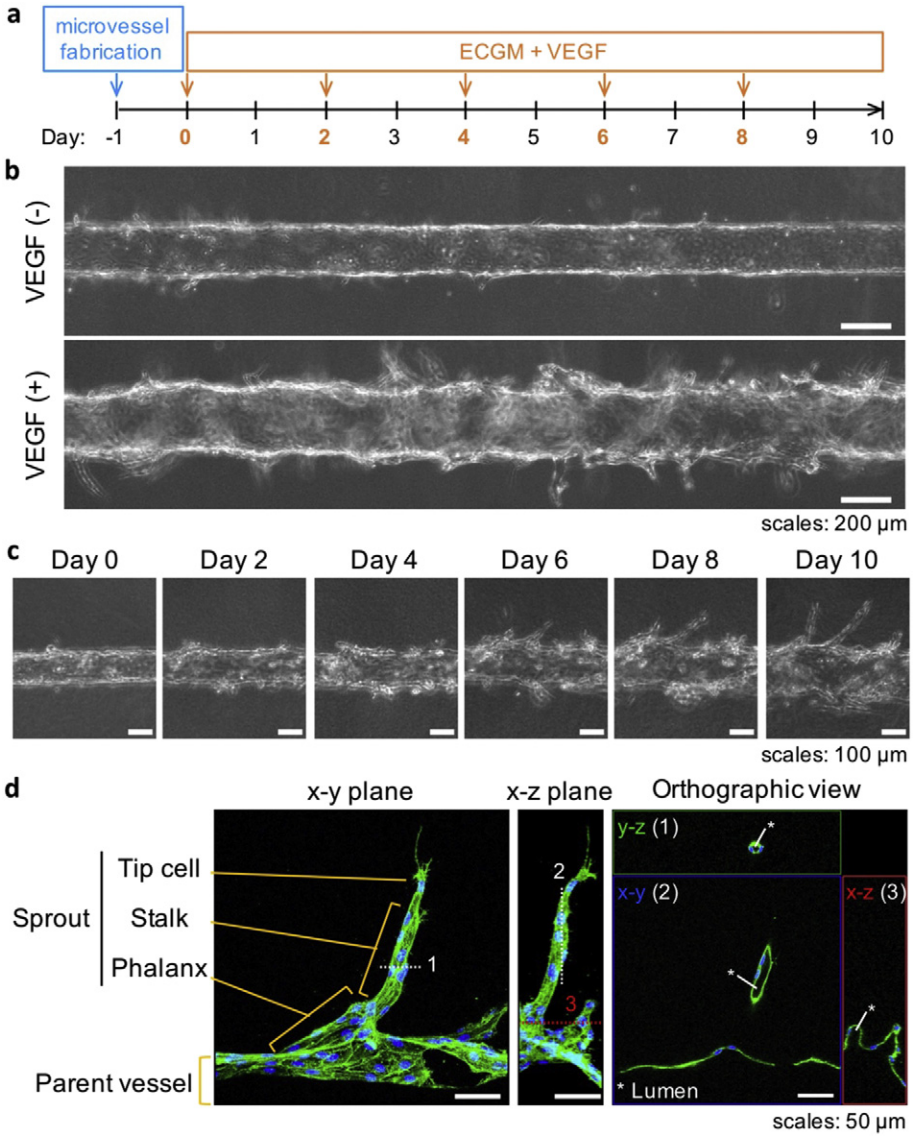

Fig. 3. VEGF-induced sprouting from the established, initial, microvessel. (a) Timeline of the method (arrows indicate media renewal). (b) Phase-contrast images showing details of microvessels treated or not with 50 ng/mL VEGF-A (day 10). (c) Time-dependent sprout formation induced by VEGF-A treatment. (d) Immunostaining of an angiogenic sprout at day 10 showing the presence of a lumen and a tip/stalk/phalanx-cell-like organization (maximum intensity projection and orthographic view of CLSM images; green: actin; blue: nucleus; the dotted lines numbered 1, 2, and 3 indicate the cutting plane lines used for the orthographic view. A video of the 3D reconstructed image is provided as Supplementary Movie 1).

invading behavior (Fig. 4a–upper right panel). When treated with VEGF-A, a similar and more pronounced migratory behavior was observed, and some sprout-like structures appeared (Fig. 4a–lower right panel).

The ability of genetically-modified HUVEC to establish cell-cell junctions in our model was then investigated. Co-immunostaining of the actin cytoskeleton and of VE-cadherin–an essential adherens-junction protein specifically expressed by endothelial cells, was performed. In order to visualize the whole structure of the microvessels, 3D imaging was performed using light sheet fluorescence microscopy (LSFM). It confirmed the observations made by using phase-contrast imaging; HUVEC-siCtl assembled into a uniform monolayer inside the collagen lumen and treatment with VEGF-A induced the formation of angiogenic sprouts of various lengths (Fig. 4b–left panel). On the other hand, HUVEC-siDLL4 failed to form a homogenous monolayer or to establish proper junctions, as highlighted by the non-homogeneous and sometimes absent VE-cadherin staining. Interestingly, LSFM also revealed that, when treated with VEGF-A, some cells formed a monolayer with adherens-junctions, as highlighted by the presence of VE-cadherin staining (Fig. 4b–right panel). We then used CLSM to better observe adherens junctions at a single-cell level. HUVEC-siCtl established adherens junctions as shown by the VE-cadherin circumferential staining (Fig. 4c–left panel). The actin cytoskeleton was also mainly localized in cell periphery in a physiological arrangement known as cortical actin (Prasain and Stevens, 2009). Upon VEGF-A treatment, the VE-cadherin staining concentrated at the cell-cell junctions, as highlighted by the thinner and brighter signal (Fig. 4c–upper left images). Its co-localization with cortical actin was also increased, suggesting stronger cell-cell junctions (Fig. 4c–lower left images). In contrast, HUVEC-siDLL4 showed only a weak VE-cadherin circumferential staining together with areas where VE-cadherin staining was absent. When treated with VEGF-A, some cells showed a strong VE-cadherin circumferential staining, while others had weak or no staining (Fig. 4c–upper right images). When cells showed VE-cadherin staining, it co-localized with cortical actin. However, cells without VE-cadherin showed an increase in actin stress fiber numbers (Fig. 4c–lower right images)–a phenomenon

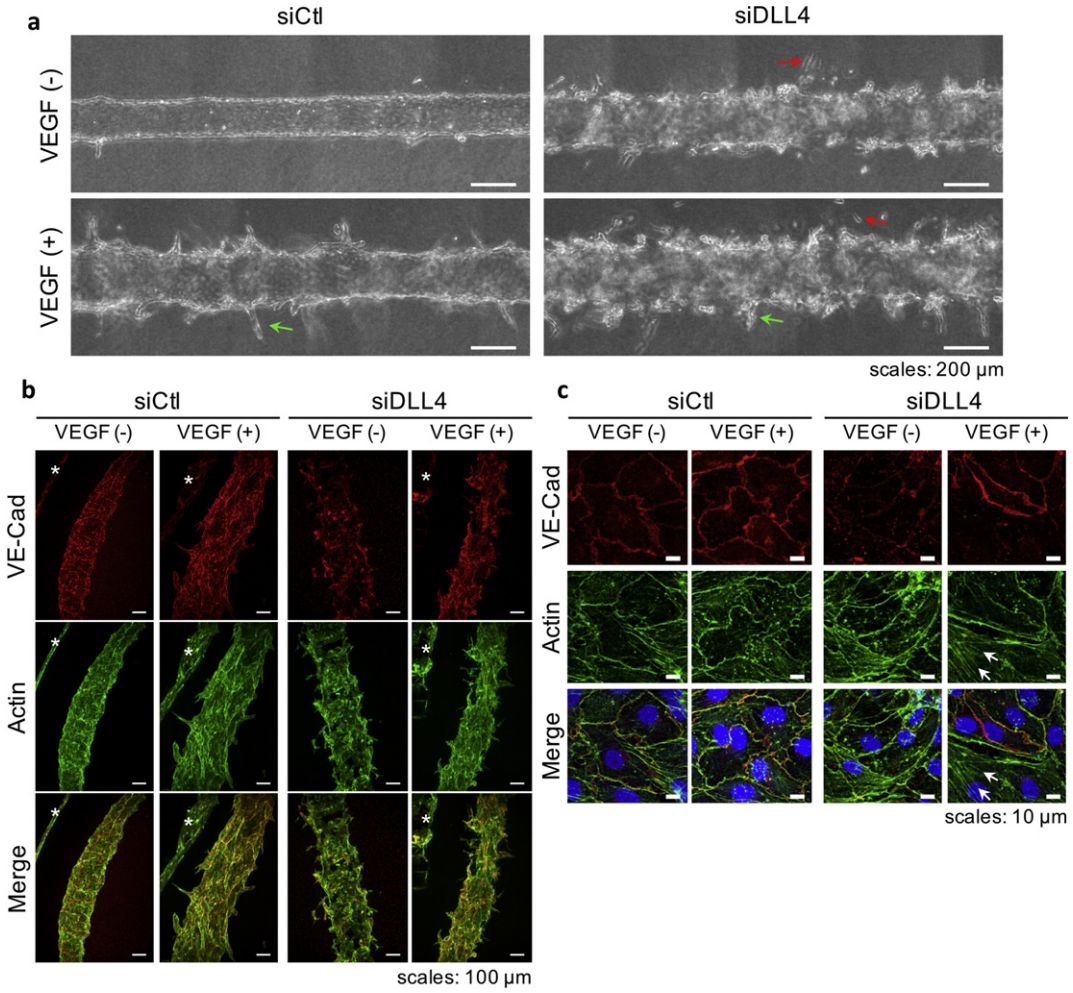

Fig. 4. Knocking-down DLL4 affects sprouting angiogenesis and microvessel integrity. (a) Phase-contrast images of microvessels made of HUVEC transfected with siControl (siCtl) or siDLL4 and treated with 50 ng/mL VEGF-A for 10 days (green arrows: sprouts, red arrows: migrating cells). (b & c) Actin and VE-cadherin (VE-Cad) immunostaining on microvessels. (b) Maximum intensity projection of LSFM 3D images showing the general morphology of microvessels (*Indicates another part of microvessel seen in background due to the LSFM method). (c) Maximum intensity projection of CLSM images showing details of the adherens-junctions and actin cytoskeleton (arrows: actin stress fibers).

observed when endothelial cells lose their cell-cell junctions and rearrange their cytoskeleton from cortical to stress fibers (Prasain and Stevens, 2009). These results confirmed previous observations that HUVEC-siDLL4 treated with VEGF-A formed a monolayer in some areas, therefore establishing cell junctions, and in other areas were isolated, therefore rearranging their cytoskeleton.

The morphology of the angiogenic sprouts was then monitored using optical coherence tomography (OCT); enabling for rapid 3D imaging without the need for immunostaining (Takahashi et al., 2017). Moreover, the 3D images could be computationally processed to model and measure isolated regions of interest. First, the obtained 3D images confirmed the effect of VEGF-A and of siRNA observed by phase-contrast microscopy and LSFM (Fig. 5a). Then, the images of HUVEC-siCtl and HUVEC-siDLL4 treated with VEGF-A were computationally processed to isolate several angiogenic sprouts, which were found in a 2-mm long area, and model them (Fig. 5b). The length, volume, surface area and average diameter of the sprouts were measured (Fig. 5c). The average length of angiogenic sprouts was similar in both conditions: 72.9 ± 27.5 µm (mean ± S.D.) for siCtl and 74.9 ± 21.3 µm for siDLL4. However, the sprouts in the siDLL4 condition showed a reduced volume compared to those of the siCtl condition. Similar observations were made regarding the surface area and the average diameter (Fig. 5c).

Taken together, these results indicate that the effective sprouting angiogenesis triggered by VEGF-A in this model depends on the Notch signaling, as reported *in vivo*.

3.3. Effects of Angiogenic Inhibitors on the In Vitro Microvessel Model

A compelling application of this model is the possibility to investigate the effects of drugs such as angiogenic inhibitors on a single molecular pathway. Aberrant angiogenesis is observed in several diseases such as rheumatoid arthritis, diabetic retinopathy and cancer. It has been proposed that targeting VEGF and its downstream signaling pathways could be of therapeutic relevance to prevent the progression of or to cure such diseases. Once VEGF-A binds to its receptor VEGFR-2, the dimerization of VEGFR-2 triggers its intracellular kinase activity, which activates several pro-angiogenic pathways (Simons et al., 2016). Sorafenib and sunitinib are kinase inhibitors targeting VEGFR-2 that have been validated as anti-angiogenic therapies currently in clinical use as treatments for metastatic renal cell carcinoma. Additionally, sorafenib is also used for treating hepatocellular carcinoma, while sunitinib is used for gastrointestinal stromal cell tumor treatment. Interestingly, although both inhibitors are designed to prevent the growth of new capillaries through similar mechanisms per their design, their effects on tumors differ. While sunitinib causes tumor shrinkage, sorafenib does not (Niu and Chen, 2010; Strumberg et al., 2005; Thomas et al., 2009). We used sorafenib and sunitinib to assess whether our model enables the analysis of angiogenic inhibitors that target the VEGF-A pathway. As a proof-of-concept, microvessels were treated with 1 µM of sorafenib or sunitinib and with or without 50 ng/mL VEGF-A (Fig. 6a). After 10 days, phase-contrast images were taken

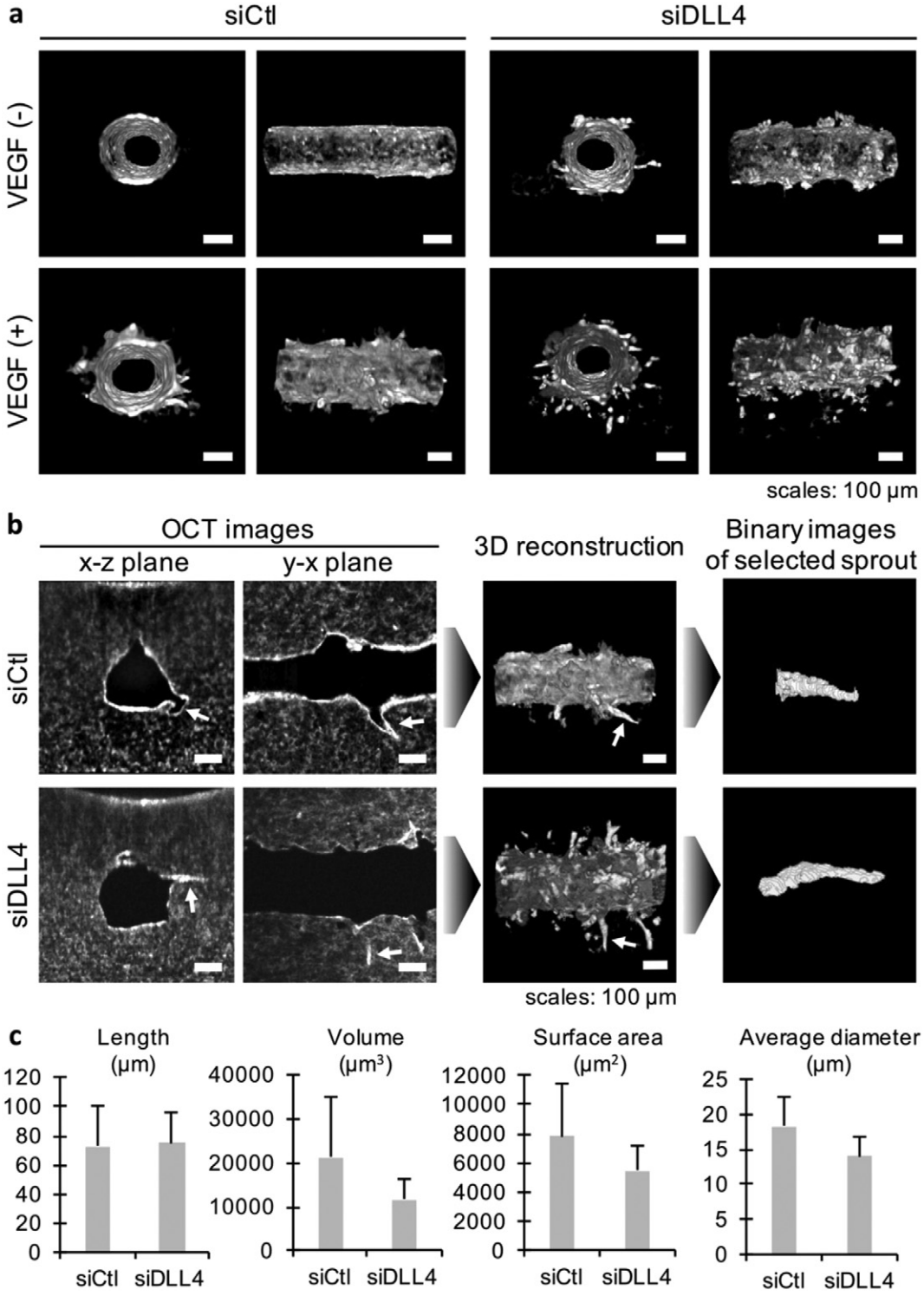

Fig. 5. Analysis of angiogenic sprouts using optical coherence tomography. (a) 3D reconstructed images of microvessels made of HUVEC transfected with siControl (siCtl) or siDLL4 and treated with 50 ng/mL VEGF-A for 10 days (lumen and side views). (b) Example of computational modeling of an angiogenic sprout of interest for measurement of its dimensions (white arrows: selected sprout). (c) Average length, volume, surface area and diameter measured from 3D binary images of angiogenic sprouts in a 2-mm-long area of microvessels treated with VEGF-A for 10 days ($n = 10$ sprouts, error bars: S.D.).

(Fig. 6b) and computationally analyzed by the directional pixel variance method (Fig. 6c) in order to quantitatively investigate the effect of inhibitors.

The directional pixel variance method was developed for this study to provide an efficient and simple way to determine how a microvessel responded to a treatment compared to a control microvessel, *i.e.*, a microvessel showing no angiogenesis and a quiescent monolayer of endothelial cells. On phase-contrast images, for each line of pixels parallel to the microvessel's longitudinal axis within a selected region, the method measures the average pixel intensity and generates a translated profile which represents the theoretical image that would be obtained if the microvessel was regular (Fig. 6c, left). This profile is then deducted from the original/input image, thus highlighting areas where the pixel intensity varies from the theory–such areas are called “residuals”. The

square of the residuals is averaged to give a quantity that can be compared between different samples (see Materials and Methods for details). A low value–low directional pixel variance–will indicate a microvessel with smooth edges, because such a microvessel will have few if any residuals. On the opposite, a high value–high directional pixel variance–will express a microvessel with rough edges, sprouts, or many cells migrating outward. In our model, sorafenib and sunitinib successfully inhibited VEGF-induced sprouting as shown by the lack of increased directional pixel variance when compared to microvessels which were not treated with VEGF-A (Fig. 6c, right). Moreover, the established microvessel was not morphologically impaired when adding the inhibitors in the absence of VEGF-A (Fig. 6b, left panel), suggesting that these inhibitors had no effect on the quiescent endothelial cells of the initial microvessel. As complementary information, a dose-dependency of the inhibition could be observed with 1 μM being the most effective dose for both inhibitors (Fig. S2).

The effects of sorafenib and sunitinib on the endothelial barrier function of the parent microvessel were also investigated because these inhibitors are known to have different effects on tumors and other targets besides VEGFR-2 (Niu and Chen, 2010). A simplified method of a previously developed permeability assay was used, in which 70 kDa fluorescein isothiocyanate (FITC)-dextran was introduced into the lumen of microvessels and extravasation of the fluorescence into collagen gel was monitored by CLSM (Pauty et al., 2017). Microvessels untreated with VEGF-A for 10 days showed an impaired barrier function, while microvessels treated with VEGF-A showed less leakage (Fig. 6d). When microvessels were treated with a combination of VEGF-A and sorafenib, the barrier function was strongly impaired as visualized by the leakage of fluorescent dye outside of the original microvessel. However, when microvessels were treated with a combination of VEGF-A and sunitinib, they were less leaky than when treated solely with VEGF-A (Fig. 6d).

Immunostaining of adherens junctions (VE-cadherin) and actin cytoskeleton of HUVEC treated in these various conditions was then performed. The microvessels not treated with VEGF-A showed holes between endothelial cells, correlating with the presence of actin stress fibers (Fig. 6e). Moreover, VE-cadherin staining was irregular in some areas. This suggested the presence of weak adherens junctions and could therefore explain the leakage observed in this condition. On the other side, the microvessels treated with VEGF-A showed a homogenous distribution of VE-cadherin concentrated at the cell edges and colocalizing with cortical actin. Interestingly, immunostaining also revealed that endothelial cells elongated and aligned along the longitudinal axis of the microvessel in this condition. This suggests that stronger adherens junctions are formed upon VEGF-A stimulation, resulting in a reduced leakage. Regarding the angiogenic inhibitors, both succeeded at inhibiting sprouting as demonstrated by phase-contrast images and directional pixel variance data (Fig. 6b & c), but leakage was not prevented when sorafenib was used (Fig. 6d). Immunostaining revealed that VE-cadherin was non-homogeneously distributed, actin stress fibers were often seen, and holes between endothelial cells could sometime be observed upon sorafenib treatment (Fig. 6e), recapitulating thus partly the observations made for the untreated microvessels. However, when using sunitinib, immunostaining showed that VE-cadherin was homogenously distributed at cell edges and colocalized with cortical actin, indicating effective adherens junctions (Fig. 6e). Noticeably, the endothelial cells did not elongate or aligned upon VEGF-A/sunitinib treatment, contrarily to VEGF-A-only treatment.

4. Discussion

Altogether, we have established here an efficient model of VEGF-induced sprouting angiogenesis which may be used to investigate the anti-angiogenic properties of candidate compounds. This model carries great potential for discovering unexpected effects of such compounds on the endothelial physiology as it enables the simultaneous analysis of sprouting angiogenesis and endothelial barrier function.

Our model is based on a human tubular endothelium embedded in a collagen matrix that mimics a parent vessel. Upon VEGF-A treatment, new capillaries sprout from the parent vessel and form a lumen in the absence of a dynamic flow. The formation of a lumen within the sprouts in the absence of hydrodynamic forces is consistent with *in vitro* and *in vivo* studies (Charpentier and Conlon, 2014) which showed that endothelial cells can form a lumen by two complementary mechanisms; namely, cell and cord hollowing. While cell hollowing consists in endothelial cells creating a lumen *via* a vacuolation process resulting in a single cell surrounding a luminal space; cord hollowing is a mechanism by which adjacent endothelial cells connected by adherens junctions first establish an apicobasal polarity before separating, redistributing their junctions and forming a luminal space between their apical sides (Charpentier and Conlon, 2014). It has been proposed that the hydrodynamic forces due to blood stream induce deformation of the apical membranes, leading to further extension of the initial lumen through a process named inverse blebbing (Gebala et al., 2016). Although further analysis is required in our model, the presence of an ECM surrounding the sprouts may provide an adequate environment for the endothelial cells to establish polarity; therefore, enabling the spontaneous lumenization by endothelial cells. Interestingly, this suggests that our model could be fit to study such phenomenon.

The VEGF-A dependency and the morphology of the sprouts suggested that the sprouts formed in this model mimicked those observed *in vivo*. In order to perform further validation at a molecular level, the study of the DLL4/NOTCH1 pathway showed that altering this pathway by RNA interference led to cells migrating into the collagen and sprouts of a smaller volume (Figs. 4 & 5). This is consistent with previous works made *in vivo* and *in vitro* on the DLL4/NOTCH1 pathway, which reported that a loss or inhibition of this pathway caused increased migration of endothelial cells and the formation of thinner vessels (Benedito et al., 2008; Lee et al., 2016; Scehnet et al., 2007). In addition to providing further validation that the model mimics *in vivo* sprouting angiogenesis, these results demonstrate that the present model enables the use of genetically-modified human primary endothelial cells to investigate the effect of gene knock-down on sprouting angiogenesis. Although we used siRNA technology, other technologies such as shRNA or a gene overexpression plasmid combined with an inducible system could be used to investigate gene functions at a specific time of angiogenesis, as a few examples.

One of the first targeted application for this model was to study angiogenic inhibitors. As a proof-of-concept, we used sorafenib and sunitinib which showed anti-angiogenic effects upon VEGF-A stimulation, thus validating the model for investigating angiogenic inhibitor molecules. Furthermore, one main advantage of our model is the presence of an established, calibrated, luminized, perfusable and imaging-compatible parent vessel. This makes fertile ground for investigating further the angiogenic inhibitors on their effects toward the parent vessel, such as the endothelial barrier function and cell-cell junctions. This is of interest as tyrosine kinase angiogenic inhibitors, although they often share a common target such as VEGFR-2, differ by other kinase targets and may therefore display effects other than only inhibiting angiogenic sprouting.

In our model, the endothelial barrier function could be studied through a permeability assay to 70 kDa FITC-dextran in combination with immunostaining of cell-cell junctions and actin cytoskeleton. In normal conditions, endothelial cells establish an effective barrier which prevents the leakage of 70 kDa FITC-dextran; therefore, it was surprising to observe leakage in the untreated microvessels (Fig. 6d). A live/dead cell staining demonstrated that HUVEC were still alive at the end of experiment (Sup. Method 3 and Fig. S2), eliminating the hypothesis that the leakage was due to dead cells. Immunostaining results suggest the presence of weak adherens junctions, contrarily to when the microvessels were treated with VEGF-A. Altogether, it is reasonable to

infer that the impaired barrier function of untreated microvessels was a result of long culture time in ECGM without VEGF-A, impeding the formation of strong cell-cell junctions. Conversely, VEGF-A is known to induce vascular permeability through the opening of adherens junctions by a VEGFR-2/VE-cadherin signaling (Gavard and Gutkind, 2006). This suggests that a balance exists between the effects of VEGF-

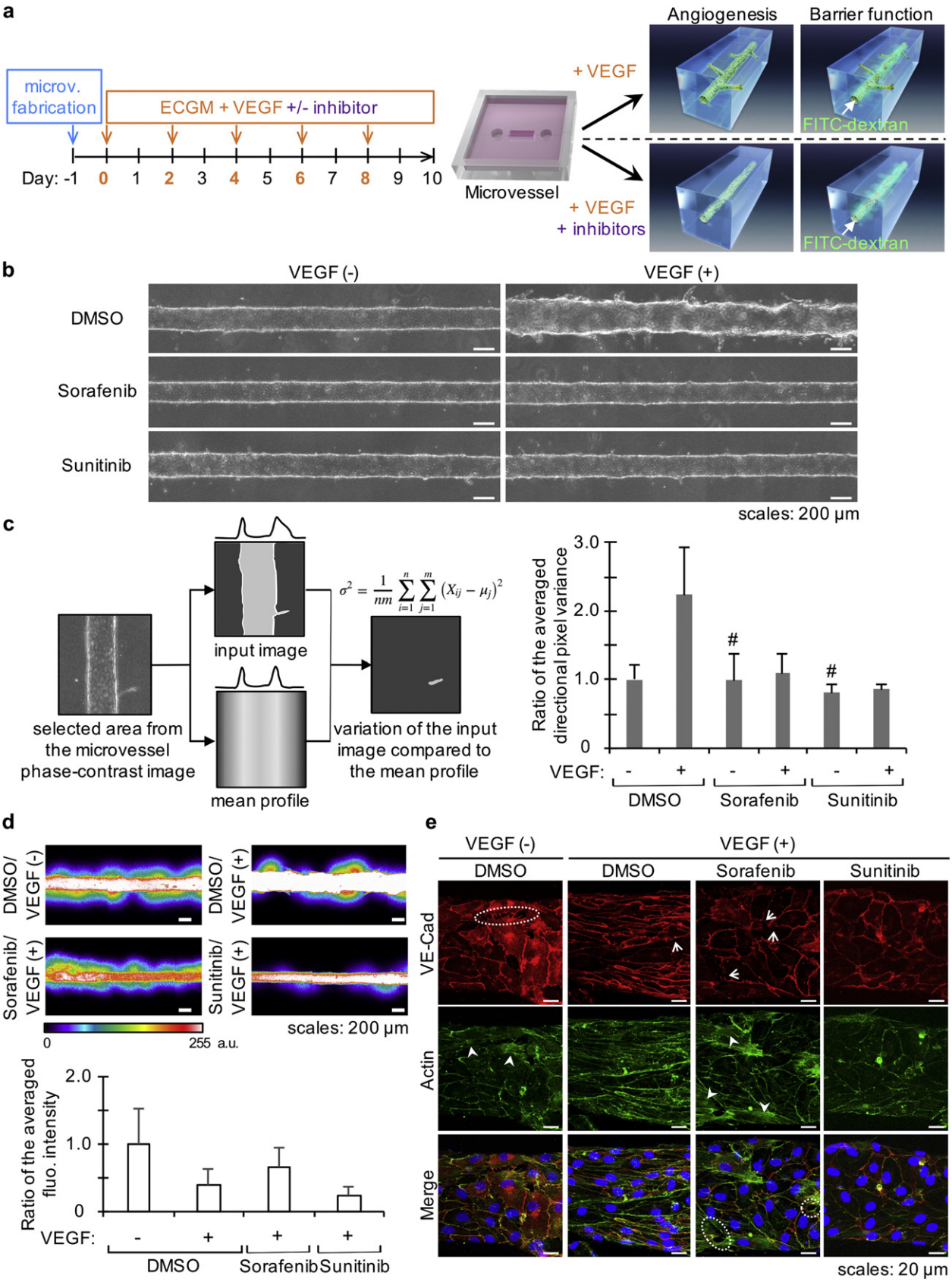

A on: (i) cell maintenance allowing for the formation of strong cell-cell junctions, and (ii) the induction of endothelial permeability *via* the opening of adherens junctions. It is illustrated by the moderate leakage observed in microvessels treated with VEGF-A (Fig. 6d). Regarding the effects of angiogenic inhibitors on permeability, the results for sorafenib recapitulated those of the untreated microvessels in spite of the presence of VEGF-A. It implies that sorafenib canceled the positive effects of VEGF-A, *i.e.* not only the induction of angiogenesis but also on permeability. This is consistent with the known effect of sorafenib on cell cycle as it was reported to have a cytostatic effect due to the inhibition of the RAF proto-oncogene serine/threonine-protein kinase (RAF1/cRAF) (Iacovelli et al., 2016; Plastaras et al., 2007; Wilhelm et al., 2004). RAF1 is an essential component of the mitogen-activated-protein-kinase (MAPK) signaling pathway that controls cell division and proliferation. The MAPK signaling pathway is one of the pathways triggered by VEGFR-2 activation, therefore sorafenib can block VEGF-A/VEGFR-2 signaling at two levels, providing an explanation for the drastic effect observed in our model. Sunitinib, on another hand, inhibited sprouting but had no effect on microvessel integrity (Fig. 6). Taken together, these results indicate that our model enables to distinguish differential effects between sorafenib and sunitinib which both target VEGFR-2 but diverge by some other targets. This is of interest for cancer treatments in the context of vascular normalization therapy (Goel et al., 2011; Carmeliet and Jain, 2011b) as sunitinib seems to normalize microvessels on two levels: (i) inhibiting abnormal angiogenesis and (ii) enabling the establishment of an effective barrier function in an environment rich in VEGF-A, such as the tumoral microenvironment. Therefore, it could explain why sunitinib led to tumor shrinkage while sorafenib did not (Niu and Chen, 2010; Thomas et al., 2009; Strumberg et al., 2005).

As mentioned in the introduction, other models using human endothelial cells have been developed. The main advantage of tissue-engineering-based model over other available technologies is the presence of an initial parent vessel that is a necessary requirement for studying angiogenesis, because it is defined as the formation of new capillaries from a pre-existing vessel. The previous works demonstrated the possibility to use such an approach to study the angiogenesis (Nguyen et al., 2013) or the barrier function/permeability (Chrobak et al., 2006). But some limitations were highlighted, *e.g.*, the cell type was changed accordingly with the analysis performed, coculture with fibroblast was required and a combination of several pro-angiogenic factors was necessary. One advantage of the *in vitro* models is the possibility to study the role of a specific factor and/or drugs targeting this factor or associated pathways. Coculture and the use of a cocktail of factors greatly weaken such advantage. Here, we demonstrated that sprouting angiogenesis may be induced from a parent microvessel solely by VEGF-A–the main inducing factor *in vivo*. Then, we could inhibit this phenomenon by using inhibitors targeting the VEGF-A receptor. As another major achievement compared to previous works, we reported the simultaneous analysis of angiogenesis and barrier function in a same microvessel, *i.e.*, only one type of cells–HUVEC–was used. This cannot be achieved by 2D models– which provide only fragmented information–and was not reported with other similar 3D models. Thanks to this simultaneous analysis, we could observe that while sorafenib and sunitinib inhibit angiogenesis similarly, they alter the barrier function of the established endothelium differently. This differential effect raises new hypotheses about the reasons behind the different outcomes observed in clinic when using these inhibitors. Furthermore, the design of the PDMS chip makes easy the perfusion of other liquid or cells within the lumen of the microvessel or the inclusion of cells into the ECM. This shall enable the study of flow on angiogenesis, and interaction between circulating immune and cancer cells and the endothelium in the context of angiogenesis. Previous works already demonstrated how such studies could be performed in quiescent microvessels (Chrobak et al., 2006; Mannino et al., 2017; Price et al., 2010) and we validated the feasibility in our model (Sup. Method 4 and Fig. S4).

Besides the various possibilities offered by our model, some limitations remain and should be addressed in future developments. First, the VEGF-A is introduced in the whole environment and does not reproduce the directionality of gradient which is naturally established *in vivo* from the hypoxic tissue. The model earns in simplicity but loses the capacity to study such directional migration of angiogenic sprouts. On another hand, the directional pixel variance method faithfully translates whether a microvessel responded to VEGF-A stimulation, and therefore can be easily used to validate angiogenic inhibitors. However, it is not effective to distinguish between migrating cells and angiogenic sprouts, therefore it is limited in its application when it comes to study gene functions, especially if the candidate gene affects cell migration. In that case, OCT analysis or videomicroscopy would be more relevant. Finally, although it is possible to study the permeability to fluorescent-labeled molecules, an analytical method to precisely measure a permeability coefficient has not yet been developed. In its current state, the method enables an easy comparison between several conditions.

In summary, we report the use of an *in vitro* 3D model of a human blood vessel for the study of VEGF-A-induced sprouting angiogenesis and angiogenic inhibitors. As a major advance, it enables the simultaneous study of angiogenesis and endothelial barrier function–two main characteristics of blood vessels that are impaired in diseases such as rheumatoid arthritis, diabetic retinopathy and cancer. The model already offers the possibility to: (i) explore gene functions through the use of genetically-modified cells, (ii) study the lumenization of new capillaries, (iii) test angiogenic inhibitors. Of relevance to translational research, this model enables the investigation of the effect of candidate molecules at a tissue level in a human-related model; as well as the description of human-specific or unanticipated effects, therefore it may contribute to reducing the number of candidate molecules which pass pre-clinical studies but fail in clinical trial. Although such technology in its current state cannot yet easily be used for preliminary screening when a high throughput is needed, it would be of value as an intermediate model between 2D cell culture models and pre-clinical animal models or complementary to the latter. Overall this technology should contribute to improve the discovery of promising anti-angiogenic molecules as well as providing a convenient tool to assess fundamental questions about mechanisms at work at an endothelial-level during VEGF-A-induced angiogenesis.

Funding Sources

This work was partly supported by the Japan Society for the Promotion of Science (JSPS) through the Core-to-Core Program and a Grant-in-Aid for JSPS Research Fellows, the Foundation for the Promotion of

Fig. 6. Inhibition of sprouting angiogenesis by sorafenib and sunitinib. (a) Timeline and schematic of the method (microv.: microvessel; arrows indicate media renewal). (b) Phase-contrast images of representative microvessels (DMSO: dimethyl sulfoxide). (c) *Left:* Conceptual model of the directional pixel variance method based on phase-contrast images for evaluating the responsiveness of microvessels to VEGF (more details are given in the text). *Right:* Results of the analysis by the directional pixel variance method showing the inhibitory effect of 1 μM sorafenib and sunitinib on microvessels treated with 50 ng/mL VEGF-A for 10 days (the bar graph shows combined data of two independent experiments, $n = 2 + 3$ microvessels but for # which indicates $n = 2$; values are expressed as a ratio of the averaged directional pixel variance for the untreated microvessels, *i.e.* DMSO/VEGF(−); error bar: S.D.). (d) Permeability assay on microvessels treated with 1 μM sorafenib, 1 μM sunitinib or 0.01% DMSO for 10 days. *Top:* CLSM images after introduction of 70 kDa FITC-dextran (a.u.: arbitrary unit). *Bottom:* Quantification of the leaked FITC-dextran from the microvessel (data shown are from one representative experiment of two independent experiments; $n = 3$ microvessels; values are expressed as a ratio of the averaged fluorescence intensity for the untreated microvessels; error bar: S.D.). (e) Actin and VE-cadherin (VE-Cad) immunostaining on microvessels treated for 10 days: maximum intensity projection of CLSM images showing details of the adherens junctions (red) and actin cytoskeleton (green); dotted lines encircle examples of region with holes between the cells, →: missing VE-cadherin, and ➤: region rich in actin stress fibers.

Industrial Science (FPIS), the Ligue Régionale contre le cancer and the SFR Cancer Lille. J.P. is an International Research Fellow of the JSPS (P15767). I-G.C. is an intern of the UTokyo Amgen Scholars Program. F.S. is Director of Research at INSERM, France.

Conflicts of Interest

Dr. Masayoshi Kobayashi and Mr. Keisuke Kato are employees of SCREEN Holdings Co., Ltd.

Author Contributions

J.P., F.S., and Y.T.M designed research. J.P., R.U., I.G.C, L.H., H.T, K.K., H.N., E.L. and F.S. performed research. J.P., L.H., K.K, M.K., and F.Y. contributed new analytic tools and analyzed data. J.P., R.U., I.G.C., L.H., F.Y., F.S., and Y.T.M. wrote the paper.

Acknowledgements

The authors thank Pr. Naoki Mochizuki (National Cerebral and Cardiovascular Center Research Institute) for his advice in LSFM, Mr. Yasuhiro Ookawa and Dr. Koji Fujimoto (Dai Nippon Printing Co., Ltd.) for their assistance in the PDMS device fabrication, Ms. Kayoko Suenaga and Mr. Kenji Minami (Carl Zeiss, GmbH) for their help with movie making, Dr. Yosuke Hiraoka (Nitta Gelatin Inc.) for his kind support in collagen preparation, Mr. Kenji Ueyama (SCREEN Holdings Co., Ltd.) for his advice regarding OCT, Ms. Eri Otsuka (University of Tokyo) for her technical assistance, and Mr. Takashi Ando for his contribution to the artwork.

Appendix A. Supplementary data

Supplementary data to this article can be found online at https://doi.org/10.1016/j.ebiom.2017.12.014.

References

Benedito, R., Trindade, A., Hirashima, M., Henrique, D., DA Costa, L.L., Rossant, J., Gill, P.S., Duarte, A., 2008. Loss of notch signalling induced by Dll4 causes arterial calibre reduction by increasing endothelial cell response to angiogenic stimuli. BMC Dev. Biol. 8, 117.

Blanco, R., Gerhardt, H., 2013. VEGF and notch in tip and stalk cell selection. Cold Spring Harb. Perspect. Med. 3, a006569.

Carmeliet, P., Jain, R.K., 2000. Angiogenesis in cancer and other diseases. Nature 407, 249–257.

Carmeliet, P., Jain, R.K., 2011a. Molecular mechanisms and clinical applications of angiogenesis. Nature 473, 298–307.

Carmeliet, P., Jain, R.K., 2011b. Principles and mechanisms of vessel normalization for cancer and other angiogenic diseases. Nat. Rev. Drug Discov. 10, 417–427.

Charpentier, M.S., Conlon, F.L., 2014. Cellular and molecular mechanisms underlying blood vessel lumen formation. BioEssays 36, 251–259.

Chrobak, K.M., Potter, D.R., Tien, J., 2006. Formation of perfused, functional microvascular tubes in vitro. Microvasc. Res. 71, 185–196.

Folkman, J., 1971. Tumor angiogenesis: therapeutic implications. N. Engl. J. Med. 285, 1182–1186.

Gavard, J., Gutkind, J.S., 2006. VEGF controls endothelial-cell permeability by promoting the beta-arrestin-dependent endocytosis of VE-cadherin. Nat. Cell Biol. 8, 1223–1234.

Gebala, V., Collins, R., Geudens, I., Phng, L.K., Gerhardt, H., 2016. Blood flow drives lumen formation by inverse membrane blebbing during angiogenesis in vivo. Nat. Cell Biol. 18, 443–450.

Geudens, I., Gerhardt, H., 2011. Coordinating cell behaviour during blood vessel formation. Development 138, 4569–4583.

Goel, S., Duda, D.G., Xu, L., Munn, L.L., Boucher, Y., Fukumura, D., Jain, R.K., 2011. Normalization of the vasculature for treatment of cancer and other diseases. Physiol. Rev. 91, 1071–1121.

Heiss, M., Hellstrom, M., Kalen, M., May, T., Weber, H., Hecker, M., Augustin, H.G., Korff, T., 2015. Endothelial cell spheroids as a versatile tool to study angiogenesis in vitro. FASEB J. 29, 3076–3084.

Hellstrom, M., Phng, L.K., Hofmann, J.J., Wallgard, E., Coultas, L., Lindblom, P., Alva, J., Nilsson, A.K., Karlsson, L., Gaiano, N., Yoon, K., Rossant, J., Iruela-Arispe, M.L., Kalen, M., Gerhardt, H., Betsholtz, C., 2007. Dll4 signalling through Notch1 regulates formation of tip cells during angiogenesis. Nature 445, 776–780.

Iacovelli, R., Verri, E., Cossu Rocca, M., Aurilio, G., Cullura, D., Santoni, M., De Cobelli, O., Nole, F., 2016. Is there still a role for sorafenib in metastatic renal cell carcinoma? A systematic review and meta-analysis of the effectiveness of sorafenib over other targeted agents. Crit. Rev. Oncol. Hematol. 99, 324–331.

Kim, S., Lee, H., Chung, M., Jeon, N.L., 2013. Engineering of functional, perfusable 3D microvascular networks on a chip. Lab Chip 13, 1489–1500.

Lee, D., Kim, D., Choi, Y.B., Kang, K., Sung, E.S., Ahn, J.H., Goo, J., Yeom, D.H., Jang, H.S., Moon, K.D., Lee, S.H., You, W.K., 2016. Simultaneous blockade of VEGF and Dll4 by HD105, a bispecific antibody, inhibits tumor progression and angiogenesis. MAbs 8, 892–904.

Mannino, R.G., Santiago-Miranda, A.N., Pradhan, P., Qiu, Y., Mejias, J.C., Neelapu, S.S., Roy, K., Lam, W.A., 2017. 3D microvascular model recapitulates the diffuse large B-cell lymphoma tumor microenvironment in vitro. Lab Chip 17, 407–414.

Nakatsu, M.N., Sainson, R.C., Aoto, J.N., Taylor, K.L., Aitkenhead, M., Perez-Del-Pulgar, S., Carpenter, P.M., Hughes, C.C., 2003. Angiogenic sprouting and capillary lumen formation modeled by human umbilical vein endothelial cells (HUVEC) in fibrin gels: the role of fibroblasts and Angiopoietin-1. Microvasc. Res. 66, 102–112.

Nguyen, D.H., Stapleton, S.C., Yang, M.T., Cha, S.S., Choi, C.K., Galie, P.A., Chen, C.S., 2013. Biomimetic model to reconstitute angiogenic sprouting morphogenesis in vitro. Proc. Natl. Acad. Sci. U. S. A. 110, 6712–6717.

Niu, G., Chen, X., 2010. Vascular endothelial growth factor as an anti-angiogenic target for cancer therapy. Curr. Drug Targets 11, 1000–1017.

Pauty, J., Usuba, R., Takahashi, H., Suehiro, J., Fujisawa, K., Yano, K., Nishizawa, T., Matsunaga, Y.T., 2017. A vascular permeability assay using an in vitro human microvessel model mimicking the inflammatory condition. Nano 1, 10.

Plastaras, J.P., Kim, S.H., Liu, Y.Y., Dicker, D.T., Dorsey, J.F., Mcdonough, J., Cerniglia, G., Rajendran, R.R., Gupta, A., Rustgi, A.K., Diehl, J.A., Smith, C.D., Flaherty, K.T., El-Deiry, W. S., 2007. Cell cycle dependent and schedule-dependent antitumor effects of sorafenib combined with radiation. Cancer Res. 67, 9443–9454.

Potente, M., Gerhardt, H., Carmeliet, P., 2011. Basic and therapeutic aspects of angiogenesis. Cell 146, 873–887.

Prasain, N., Stevens, T., 2009. The actin cytoskeleton in endothelial cell phenotypes. Microvasc. Res. 77, 53–63.

Price, G.M., Wong, K.H., Truslow, J.G., Leung, A.D., Acharya, C., Tien, J., 2010. Effect of mechanical factors on the function of engineered human blood microvessels in microfluidic collagen gels. Biomaterials 31, 6182–6189.

Ribatti, D., Crivellato, E., 2012. "Sprouting angiogenesis", a reappraisal. Dev. Biol. 372, 157–165.

Scehnet, J.S., Jiang, W., Kumar, S.R., Krasnoperov, V., Trindade, A., Benedito, R., Djokovic, D., Borges, C., Ley, E.J., Duarte, A., Gill, P.S., 2007. Inhibition of Dll4-mediated signaling induces proliferation of immature vessels and results in poor tissue perfusion. Blood 109, 4753–4760.

Simons, M., Gordon, E., Claesson-Welsh, L., 2016. Mechanisms and regulation of endothelial VEGF receptor signalling. Nat. Rev. Mol. Cell Biol. 17, 611–625.

Staton, C.A., Stribbling, S.M., Tazzyman, S., Hughes, R., Brown, N.J., Lewis, C.E., 2004. Current methods for assaying angiogenesis in vitro and in vivo. Int. J. Exp. Pathol. 85, 233–248.

Strumberg, D., Richly, H., Hilger, R.A., Schleucher, N., Korfee, S., Tewes, M., Faghih, M., Brendel, E., Voliotis, D., Haase, C.G., Schwartz, B., Awada, A., Voigtmann, R., Scheulen, M.E., Seeber, S., 2005. Phase I clinical and pharmacokinetic study of the Novel Raf kinase and vascular endothelial growth factor receptor inhibitor BAY 43-9006 in patients with advanced refractory solid tumors. J. Clin. Oncol. 23, 965–972.

Takahashi, H., Kato, K., Ueyama, K., Kobayashi, M., Baik, G., Yukawa, Y., Suehiro, J.I., Matsunaga, Y.T., 2017. Visualizing dynamics of angiogenic sprouting from a three-dimensional microvasculature model using stage-top optical coherence tomography. Sci. Rep. 7, 42426.

Thomas, A.A., Rini, B.I., Lane, B.R., Garcia, J., Dreicer, R., Klein, E.A., Novick, A.C., Campbell, S.C., 2009. Response of the primary tumor to neoadjuvant sunitinib in patients with advanced renal cell carcinoma. J. Urol. 181, 518–523 (discussion 523).

Tourovskaia, A., Fauver, M., Kramer, G., Simonson, S., Neumann, T., 2014. Tissue-engineered microenvironment systems for modeling human vasculature. Exp. Biol. Med. 239, 1264–1271.

Wilhelm, S.M., Carter, C., Tang, L., Wilkie, D., Mcnabola, A., Rong, H., Chen, C., Zhang, X., Vincent, P., Mchugh, M., Cao, Y., Shujath, J., Gawlak, S., Eveleigh, D., Rowley, B., Liu, L., Adnane, L., Lynch, M., Auclair, D., Taylor, I., Gedrich, R., Voznesensky, A., Riedl, B., Post, L.E., Bollag, G., Trail, P.A., 2004. BAY 43-9006 exhibits broad spectrum oral antitumor activity and targets the RAF/MEK/ERK pathway and receptor tyrosine kinases involved in tumor progression and angiogenesis. Cancer Res. 64, 7099–7109.

Yokota, Y., Nakajima, H., Wakayama, Y., Muto, A., Kawakami, K., Fukuhara, S., Mochizuki, N., 2015. Endothelial Ca 2 + oscillations reflect VEGFR signaling-regulated angiogenic capacity in vivo. elife 4.

Zheng, Y., Wang, S., Xue, X., Xu, A., Liao, W., Deng, A., Dai, G., Liu, A.P., Fu, J., 2017. Notch signaling in regulating angiogenesis in a 3D biomimetic environment. Lab Chip 17, 1948–1959.